Soft Matter

PAPER

Cite this: *Soft Matter*, 2016, **12**, 6430

Anisotropic magnetoresistivity in structured elastomer composites: modelling and experiments

José Luis Mietta,[a] Pablo I. Tamborenea[b] and R. Martin Negri*[a]

Received 21st May 2016,
Accepted 3rd July 2016

DOI: 10.1039/c6sm01173j

www.rsc.org/softmatter

A constitutive model for the anisotropic magnetoresistivity in structured elastomer composites (SECs) is proposed. The SECs considered here are oriented pseudo-chains of conductive-magnetic inorganic materials inside an elastomer organic matrix. The pseudo-chains are formed by fillers which are simultaneously conductive and magnetic dispersed in the polymer before curing or solvent evaporation. The SEC is then prepared in the presence of a uniform magnetic field, referred to as $\mathbf{H}_{curing}$. This procedure generates the pseudo-chains, which are preferentially aligned in the direction of $\mathbf{H}_{curing}$. Electrical conduction is present in that direction only. The constitutive model for the magnetoresistance considers the magnetic pressure, P_{mag}, induced on the pseudo-chains by an external magnetic field, H, applied in the direction of the pseudo-chains. The relative changes in conductivity as a function of H are calculated by evaluating the relative increase of the electron tunnelling probability with P_{mag}, a magneto-elastic coupling which produces an increase of conductivity with magnetization. The model is used to adjust experimental results of magnetoresistance in a specific SEC where the polymer is polydimethylsiloxane, PDMS, and fillers are microparticles of magnetite–silver (referred to as Fe_3O_4[Ag]). Simulations of the expected response for other materials in both superparamagnetic and blocked magnetic states are presented, showing the influence of the Young's modulus of the matrix and filler's saturation magnetization.

1 Introduction

Magnetic composites formed by dispersions of magnetic fillers into an organic matrix are receiving increasing attention because of the possibilities of observing very large magnetoresistive effects with moderate magnetic field intensities.[1–5] Pioneering systematic research on magnetorheology and anisotropic effects was reported by the group of Zrinyi[6–8] and by Nikitin and co-authors.[9–11] The most common matrices are viscous gels or elastomer polymers while fillers can be isotropic or anisotropic dispersions of magnetic particles. In particular, the composites formed by anisotropic dispersions in an elastomer matrix are referred to as structured elastic composites (SECs), which are easily formed by preparing the elastic material under the application of a uniform magnetic field. For instance, if the magnetic particles are dispersed in polydimethylsiloxane (PDMS) when the polymer is still fluid, and then thermal curing is performed under a magnetic field $\mathbf{H}_{curing}$, the final cured system is a SEC because the magnetic particles group together forming several chains inside the matrix, and are preferentially oriented in the direction of $\mathbf{H}_{curing}$.[2,3,12–17] Another example is the case of a polymer dissolved in a volatile solvent, for example styrene-butadiene rubber (SBR) in toluene, in which the magnetic fillers are incorporated and then the solvent is completely evaporated in the presence of a magnetic field.[15] These systems, and also those based on fluid gels, present magnetoresistivity, that is, the change in the electrical resistance by an external magnetic field, H (note that the field H must be distinguished from $\mathbf{H}_{curing}$). To observe these effects, fillers which are not only magnetic but ohmic conductors have also been used. Piezoresistivity, *i.e.* the change in the electrical resistivity with a mechanical stress, has been reported in those systems.[2,3,12–14] In particular, in the case of elastic materials, it is possible to obtain sensors of the magnetic field (exploiting the magnetoresistivity) and/or of mechanical stress (based on the piezoresistivity). Besides, when using SECs, the response of those sensors is anisotropic and conditions can be matched to obtain an electrical signal only when the external fields are applied in the direction of the structure. Most of the SECs are constituted by several inorganic chains inside the organic elastomer. The chains are referred to as pseudo-chains since they are complex agglomerations of the magnetic particles, presenting fractures and polymer interpenetration which are formed during preparation. The pseudo-chains are preferentially aligned in the direction of $\mathbf{H}_{curing}$ (with an angular dispersion) and form columns that can extend across millimeter slides of the material, generating connectivity

[a] *Instituto de Química Física de Materiales, Ambiente y Energía (INQUIMAE), Departamento de Química Inorgánica, Analítica y Química Física, Facultad de Ciencias Exactas y Naturales, Universidad de Buenos Aires, Argentina. E-mail: rmn@qi.fcen.uba.ar; Fax: +54-11-4576-3341; Tel: +54-11-4576-3358*

[b] *Departamento de Física and Instituto de Física de Buenos Aires (IFIBA), Facultad de Ciencias Exactas y Naturales, Universidad de Buenos Aires, Argentina*

(conduction) from one face to the other of the slide in the direction of $\mathbf{H}_{curing}$. If the percentage of particles in the material is too low, there is no connectivity between opposite faces: there is no percolation between pseudo-chains and the SEC behaves as an insulator. In the other extreme, if the percentage of particles is too high, and if instrumental factors such as intensity of $\mathbf{H}_{curing}$ and time of exposition to the field are not optimized, then pseudo-chains present a large angular dispersion and hence connectivity not only in the direction of $\mathbf{H}_{curing}$ but also perpendicular to the field can be obtained, that is, there is percolation in more than one direction. Then, under fixed instrumental conditions, there is a concentration window for which connectivity through the SEC is obtained, and then electrical conducting, only in the direction of $\mathbf{H}_{curing}$. These systems present total electrical anisotropy and that condition is referred to as TEA.[12,13] The systems and conditions we have prepared and studied in previous works are SECs, with oriented pseudo-chains formed by agglomerations of particles which are simultaneously magnetic and conductive, and presenting TEA. In a previous article[13] a model for the piezoresistivity response of those SECs was reported. The model is based on the coupling between the elastic properties of the material and the probability for electron tunnelling between regions separated by polymer interpenetration in the pseudo-chains and at its edges. That process is the limiting factor for conduction and the piezoresistive model considers the decrease of the average distance for electron tunnelling when the SEC is compressed by an external stress applied in the direction of the pseudo-chains.

These systems display not only piezoresistivity but also magnetoresistivity. The anisotropic magneto-elastic behaviour of ferrogels was modelled by Wood *et al.*[18] The interaction between magnetic particles connected through a polymer chain was simulated by Pessot and co-authors.[19] The same group used molecular dynamic simulations to study the polymer-magnetic chain interaction and its influence on the magneto-elastic properties.[20,21] Two models accounting for magnetoresistance effects in magnetic composites have been reported, to the best of our knowledge, by Kchit and co-workers[5] and Bica.[1] The SEC modelled by Kchit and co-workers is not formed by pseudo-chains but instead the fillers are organized as strings of pearls, without an internal structure, where each pearl is consecutively ordered and represents a particle, separated from each other by a thin layer of the polymer. A model for systems based on pseudo-chains requires a different approach than a model for the string of pearls. For example, the model required for systems formed by pseudo-chains needs to consider the length, diameter and relative orientation of the pseudo-chains. Factors like the electrical resistance of the pearls are not considered in the work of Kchit *et al.* since pearls appear as perfect conductors, but in our model those factors must be included. Additionally, in the string of pearls systems some specific parameters must be previously estimated, such as the thickness of the polymer layer between pearls and the surface roughness of the filler (the last is actually given by four roughness parameters experimentally estimated). It appears that string of pearls systems can be more easily formed in matrices with relatively low degree of cross-linking. The other model is the one developed by Bica, which was used to fit the magnetoresistive response of a composite whose matrix is silicon oil instead of an elastomer; hence, the matrix is modelled as a viscous fluid, incorporating the friction exerted by the matrix on the filler particles, with point-magnetic dipole interaction between fillers. The viscous system studied by Bica is very different from the elastic composite investigated here, and therefore his model is not applicable to the description of the magnetoresistive response in our SEC. Recently, Ivaneyko *et al.*[22] reported a formalism for the magnetostriction effect (*i.e.* magneto-induced deformation) in SEC systems, which can be used to model the magnetoresistive response of those systems. In the Ivaneyko *et al.* model, the SEC is not formed by pseudo-chains but rather by a three-dimensional periodic arrangement of particles with an anisotropic distribution inserted in the matrix. Even after making suitable changes to the model in order to adapt it to our systems, we found that it was not able to fit our experimental data satisfactorily. We observed that the Ivaneyko's model underestimates the magnetoresistance effects in SECs formed by pseudo-chains, perhaps because the interactions between complex structures like pseudo-chains cannot be well accounted by point-dipole magnetic interactions, as described by Ivaneyko *et al.* It is worth highlighting that none of these models take into account the condition of TEA.

Thus, the aim of the present work is to present a constitutive model for magnetoresistivity in SECs formed by magneto-conductive pseudo-chains under TEA conditions. Within that frame, the main issue to be addressed is the origin of the large magnetoresistive effects observed in SECs. Although the model is applicable to any kind of SEC, the experimental procedure we use to obtain SECs is described here. First, magnetic nanoparticles (NPs) are synthesized. Currently we use NPs which are in the superparamagnetic regime at room temperature in order to avoid irreversibility in the magnetoresistive response, but the case of NPs in blocked states is considered in the present work also. The magnetic NPs form agglomerates because of the magnetic interactions between them. Then, silver (Ag) is reduced on those agglomerates forming microparticles (μPs) which are simultaneously magnetic and electrically conductive. These μPs, here referred to as NPs[Ag], are dispersed in the elastomer and then the composite is cured in the presence of $\mathbf{H}_{curing}$. In this way, several NPs[Ag] microparticles form one pseudo-chain and several pseudo-chains align and percolate forming several columnar structures in the direction of $\mathbf{H}_{curing}$. The model developed in the present work applies to all these systems as long as TEA can be obtained. One of the SECs used in previous works (Fe_3O_4[Ag]–PDMS 4.2% v/v of μPs) is here referred to as the reference SEC and taken as a reference material to present connections between the theoretical parameters and its experimentally observed magnitudes, helping to choose realistic parameters of the SEC when simulating magnetoresistive responses. The magnetoresistivity of the reference SEC was fit using the developed model.

2 Materials and methods

2.1 Preparation of Fe_3O_4[Ag]–PDMS SEC material

The preparation method used to obtain the Fe_3O_4[Ag]–PDMS SEC was described in detail in our previous articles[2,3,14] This procedure

is briefly described here. First, Fe_3O_4 superparamagnetic nanoparticles (NPs) were synthesized by the chemical co-precipitation method, dropping a solution mixture (2 : 1) of $FeCl_3 \cdot 6H_2O$ and $FeCl_2 \cdot 4H_2O$ in chlorhydric acid, into a NaOH solution at pH = 14 and 60 °C, under a nitrogen atmosphere and high-speed stirring. The obtained material was subjected to repeated centrifugation–washing cycles and then dried in a vacuum oven at 40 °C for 24 h. The obtained dark brown NPs show a size distribution (determined by TEM images) with a maximum at 13 nm in the log-normal distribution of diameters, which is in excellent agreement with the size of the crystallite domains calculated using the Debye–Scherrer relation from X-ray diffractograms (XRD), (14 ± 2) nm.[3] In a second step, clusters of Fe_3O_4 NPs were covered with silver in order to obtain microparticles which are not only magnetic but electrically conductive also. For that, aqueous dispersions of $Ag(NH_3)_2^+$ and Fe_3O_4 NPs in a 10 : 1 molar ratio were sonicated for 30 minutes at room temperature. Then the system was heated in a water bath at 50 °C for 20 minutes with slow stirring. In the next step, 0.4 M glucose monohydrate solution was added drop-by-drop to the Fe_3O_4–Ag^+ suspension. Stirring was continued for one hour. This synthesis protocol promotes the reduction of Ag(I) ions adsorbed onto Fe_3O_4 particles. The magnetite–silver particles were separated out from the solution by magnetization and then by centrifugation. After the particles were separated, the decanted supernatant liquid was fully transparent. The obtained system (here referred to as Fe_3O_4[Ag]) is actually formed by microparticles whose internal structure consists of several Fe_3O_4 nanoparticle clusters covered by metallic silver grouped together. For the Fe_3O_4[Ag] microparticles (μPs) the maximum of the diameter distribution is at 1.3 μm (determined by SEM and TEM images). Finally PDMS base and a curing agent, referred to as PDMS from now on (Sylgard 184, Dow Corning), were mixed in proportions of 10 : 1 (w/w) at room temperature and then loaded with the Fe_3O_4[Ag] microparticles. The still fluid samples were incorporated into a specially designed cylindrical mould (1 cm diameter × 1.5 cm thickness) and placed in between the magnetic poles of a Varian Low Impedance Electromagnet (model V3703), which provides highly uniform steady magnetic fields. The mould was rotated at 30 rpm to preclude sedimentation and heated at (75 ± 5) °C in the presence of a uniform magnetic field ($\mu_o \mathbf{H}_{curing}$ = 0.35 Tesla) for 3 hours to obtain the cured material (Fig. 1). Control samples, prepared without applying the magnetic field, were also obtained. More details are provided in reference articles.[2,3,14,16,17] Slices of the cured composites were held in an *ad-hoc* sample-holder and cut using a sharp scalpel, obtaining slices of 2.5 mm thickness and 0.8 cm^2 area (1 cm diameter). Along this work, PDMS refers to the elastomeric matrix formed by a base : cross-linker of 10 : 1 weight ratio.

2.2 Measuring the magnetoresistive (MR) response of the SEC

Our group has reported completely reversible (without hysteresis) magnetoresistivity, MR, for SECs of Fe_3O_4[Ag]–PDMS loaded with 4.2% and 12.6% v/v of μPs.[3] The measurements of the electrical resistance, R, as a function of the magnetic field intensity, H, were performed on SEC cylindrical samples of 1 cm diameter and 2.5 mm length. These SEC samples were located between two gold electrodes connected to a potentiostat. This set-up was placed between two large electro-magnets that allow applying a uniform magnetic field in the central region between them, where the set-up was located. To ensure good electrical contact between the sample and gold electrodes, an initial stress, $P^* \approx 75$ kPa, was applied. For each H, the electrical resistance at fixed potential V = 1000 mV, and the characteristic I–V curves were measured (dc in the range ±3000 mV). The applied magnetic field, H, was measured using a Gaussmeter (Group3 DTM-133 digital Teslameter). The stabilization of the magnetic field, when it is changed from a given value to another, occurs in about 1–2 seconds (these values are actually given by the time response of the gaussmeter). When the magnetic field is changed, the electrical resistance of the SEC, R, starts to change and it is registered as a function of time until reaching a stable value. The characteristic transient

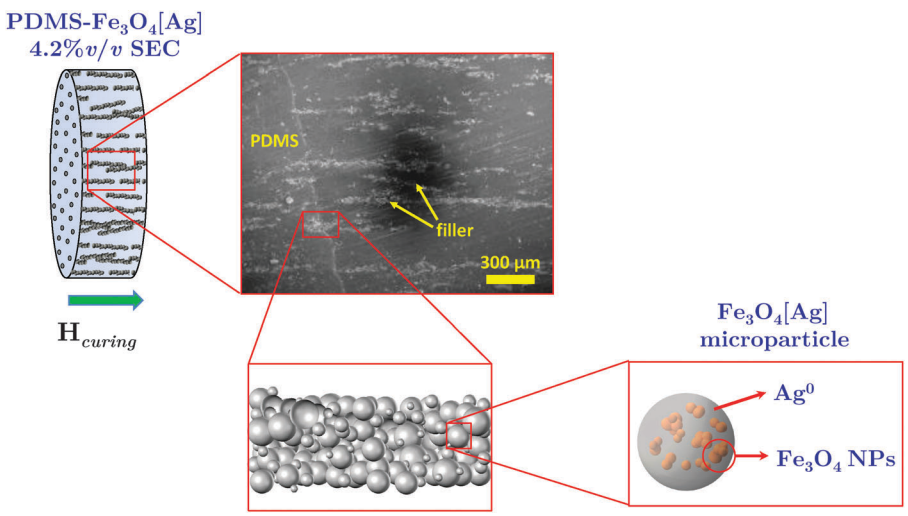

Fig. 1 Internal structure of the prepared SEC sample, mentioned as the reference SEC throughout the text. The image corresponds to a SEM micrography, where the 'filler' indicates pseudo-chains formed by Fe_3O_4[Ag] microparticles.

time for the resistance to reach stabilization is about 5–30 seconds (depending on the specific values of H and P^*), therefore a time between measurements about two minutes was considered in order to ensure that the system reaches total relaxation. Note that the transient time for full stabilization of R is much larger than that for the stabilization of H, and hence it is not related to instrumental factors mainly but to relaxation processes in the bulk of the SEC.

I–V curves were measured using a potentiostat (TEQ 4, Argentina) and magnetization curves were measured using a LakeShore 7400 Vibrating Sample Magnetometer (VSM).

3 Model

3.1 Circuital formalism

It is assumed that the powder concentration of the filler is such that conductive columns are generated in the matrix, aligned in one direction (with a small angular dispersion). It is also assumed that there is percolation between those pseudo-chains, thus connecting the opposite faces of the SEC, but there is no percolation in the direction perpendicular to the columns. In other words, the experimental conditions ensure the TEA condition. At this point it is important to mention that a mechanism based on further rotation and alignment of pseudo-chains induced by the applied field H is not expected to be an appropriate description of the magnetoresistivity. First, for systems that are in the superparamagnetic regime, the net magnetic moment induced by H, μ, is parallel to H. A further increase of H does not change the direction of μ which remains parallel to H always. Therefore, the torque between H and μ is null and there is no driving force for the rotation of pseudo-chains under application of H in the superparamagnetic regime. Second, for systems in the blocked state, where a torque may be present, it is not obvious that a rotation of pseudo-chains under application of H produces a decrease of the distance between the head and tail of two consecutive pseudo-chains. Moreover, that distance can increase after a rotation if the rotation centers of both pseudo-chains are shifted one with respect to the other. In that case the conductivity is expected to decrease under the application of H, the opposite to observations. This decrease of the effective connectivity under rotation has been reported in experimental and theoretical studies.[23–26]

Therefore, when considering the internal structure of the filler material described in the Introduction, the electrical resistance of the SEC has three main components: (i) the electrical resistance associated with the electron tunnelling between two conductive filler regions separated by an insulating layer (polymer matrix), R_{tunnel}, (ii) the electrical resistance of each one of these conductive regions, R_{CR}, and (iii) the electrical-contact resistance between conductive regions and gold electrodes, $R_{\text{E–CR}}$. Thus, the electrical resistance of the SEC samples can be described in circuital terms by a simple expression which corresponds to an equivalent circuit of N parallel resistances:[13]

$$R(P_{\text{mec}}, H) = \frac{n-1}{N} R_{\text{tunnel}} + \frac{n}{N} R_{\text{CR}} + \frac{2}{N} R_{\text{E–CR}} \qquad (1)$$

where H is the applied magnetic field, P_{mec} is the applied mechanical stress, N is the number of columnar structures that connect the electrodes and n is the number of conductive regions in each of the said columnar structures. In this way, there are $n-1$ tunnel steps in each of the columnar structures. In the formalism developed in this paper we assume that the reorganization of the filler by application of H does not change neither N nor n.

In the case of the reference SEC, Fe_3O_4[Ag]–PDMS 4%, it was estimated that N = 660 by SEM micrographs (FESEM, Zeiss Supra 40 Gemini), while n = 98 was recovered by modelling the piezoresistive response.[13] Clearly N depends on the area of the SEC sample, A, while n depends on the length of the SEC sample at null stress, L_o. In particular, for measurements made on the reference SEC, A = 0.8 cm^2 and L_o = 2.5 mm. It should be clear that N is not the number of pseudo-chains but the number of percolating columns (each column is formed by many pseudo-chains). The influence of the magnetic field on each of the terms of eqn (1) is evaluated here below.

3.1.1 Resistance between pseudo-chains and metallic electrodes $\left(\frac{2}{N}R_{\text{E–CR}}\right)$. The currently used metallic electrodes, mainly gold electrodes, are not magnetized by application of H. Therefore it is assumed in the present model that the electrode/pseudo-chain electrical contact resistance does not change by application of magnetic fields. Then, the value of $R_{\text{E–CR}}$ under the conditions of the magnetoresistive response measurement can be estimated using the Holm's model.[13,27] For instance, in the case of the reference SEC (Fe_3O_4[Ag]–PDMS) the electrical resistivity of the filler can be estimated as the electrical resistivity of metallic silver, $\rho_{\text{Ag}} \sim 10^{-8}$ Ωm. Then, using the electrical resistivity of the electrodes, $\rho_{\text{Au}} \sim 10^{-8}$ Ωm, the hardness of the filler, $\mathscr{H}_{\text{Ag}} \sim 10^2$ MPa,[28] and the average diameter of the pseudo-chains, $\langle D \rangle \sim 10$ μm,[13] it is estimated that $\frac{2}{N}R_{\text{E–CR}} \sim 10^{-4}$ Ω. Then, for the reference SEC the contribution of the electrical contact resistance is negligible. This result is generalized to any material, thus the model assumes that the electrical contacts have no appreciable contribution to the magnetoresistive response of SECs.

3.1.2 Resistance between particles that are not separated by a layer of the polymer $\left(\frac{n}{N}R_{\text{CR}}\right)$. The next step is to evaluate both the absolute contribution of R_{CR} to R and also the possible dependence of R_{CR} with H. R_{CR} is the electrical resistance of each conductive region (*i.e.* each aggregate of microparticles inside a pseudo-chain). Each one of these aggregates is separated from the next one by a polymeric layer. Inside an aggregate, a particle can be in direct contact with another, or be separated from it. In the case of the reference SEC, the resistance R_{CR} represents the resistance of an aggregate of Fe_3O_4[Ag] microparticles which are inside a pseudo-chain. For that system, the representation for the electrical flux through a single aggregate is the jump or tunnelling of electrons from regions containing silver in the microparticle A to regions containing silver in microparticle B. Those regions in microparticles A and B are assumed to be in close contact and without a polymer layer between them. For that reason it is

reasonable to expect the following: (i) the effective distance for electron jump or tunnelling between those microparticles does not vary when a magnetic field H is applied, and thus elastic or plastic deformations of the composite due to magnetic pressures induced by H are not expected to have an influence on R_{CR}, and (ii) magnetoresistance effects due to electron spin polarization do not contribute since particles A and B are not distinguishable.

The last effect, electron spin polarization, is clarified. There are reports of spin polarization effects in superparamagnetic systems[29] and few for nanocomposites.[30–35] These effects can occur between two particles if the degree of electron spin polarization is different (heterogeneous junction). The idea of the mechanism is as follows. First, it is known from spintronics that the barrier for electron tunnelling from particle A to particle B decreases when decreasing the difference in spin polarization between them since electron tunnelling is favoured when the electrons do not change their spin state. As the magnetic field H tends to polarize the electron spins, then, if A and B were of different chemical nature, the eventual difference in spin polarization between both should decrease with H with the consequent decrease of the electron tunnelling barrier and decrease of R_{CR}. For that mechanism to occur it is necessary to have a difference in the electron spin polarization between A and B, which is not the case of the SEC studied here, because microparticles A and B are indistinguishable from the point of view of their chemical composition and morphological characteristics. That is, no H-dependent electron spin polarization effects on the electrical conduction are expected since no hetero-junctions are present. Note that a hetero-junction can be present if asymmetric surface defects for particles A and B appear. For example, when silver oxides are formed with oxygen vacancies. The presence of surface defects and their contribution to the magnetoresistivity through spin-polarization effects is considered to be negligible and not taken into account in the model.

From the above considerations, possible magnetoresistance effects on R_{CR} are not included in the present model. Nevertheless, this hypothesis was experimentally tested for the Fe_3O_4[Ag] microparticles by measuring the electrical conductivity of the powders of Fe_3O_4[Ag] microparticles under different compressions and external magnetic fields. The implemented set-up for measuring the electrical conductivity of powders is diagrammed in Fig. 2(a), which is very similar to that used by Montes *et al.*[36] *I–V* characteristic curves in Fig. 2(b) show that the electrical response of Fe_3O_4[Ag] powders is ohmic for all compressions and magnetic fields. The electrical resistance decreases when the powder is compressed [see Fig. 2(b) and (c)]. This can be justified in terms of the formation of percolative paths in which electric current can flow from one electrode to the opposite.[37–39] During decompression, the electrical resistance increases, but remains at low values, possibly due to irreversible plastic deformation of the filler particles during compression.[37,39]

Fig. 2(d) shows that the application of an external magnetic field does not modify the electrical resistivity of the filler powder for none of the compressions used, as expected based on the considerations discussed above. Note also that in the reference SEC the application of a magnetic field perpendicular to the electric flow has no magnetoresistive effect.[3] In this case,

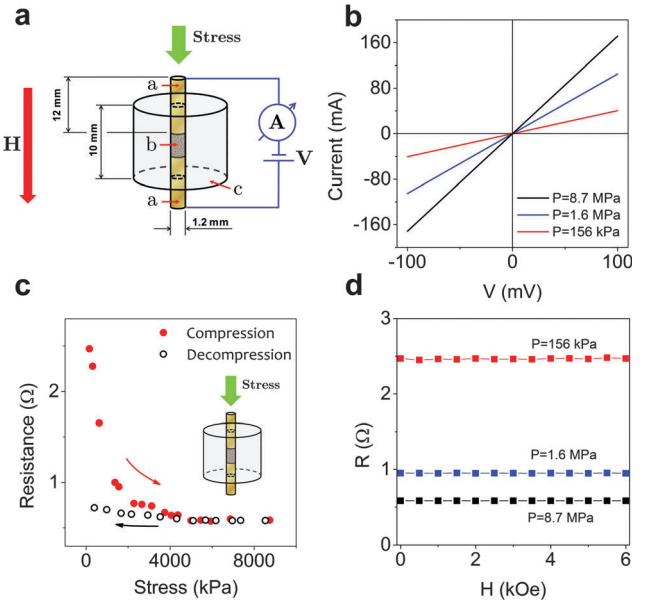

Fig. 2 (a) Set-up used to evaluate the effect of magnetic field on the electrical resistance of filler powder Fe_3O_4[Ag]: a – cylindrical copper electrodes. b – Filler powder. c – Acrylic resin container. (b) *I–V* characteristic curves at different compressions for the filler powder Fe_3O_4[Ag] (this powder was used later in the reference SEC). (c) Electrical resistance of Fe_3O_4[Ag] powder under compression–decompression cycles. (d) Magnetic field effect on the electrical resistance of the filler powder at different compressions.

the application of the magnetic field still polarizes the electronic spins,[40–42] but no change in R with H is observed. This fact is again in agreement with the hypothesis of neglecting spin polarization effects in the SEC. Therefore, no contribution of the term $\frac{n}{N}R_{CR}$ to the magnetoresistive effect is expected nor included in the model. This assumption is generalized to any magnetic particle used as a filler [its contribution to the total electrical resistance, R, for the reference SEC can be obtained from the piezoresistive response (see Mietta *et al.*[13]), which gives a value of $\frac{n}{N}R_{CR} \sim 0.5\ \Omega$].

3.1.3 Main contribution to the magnetoresistance effect (R_{tunnel}). Based on the above analysis, the developed model assumes that the main contribution to the magnetoresistance is due to R_{tunnel}. In our previous work we showed that the generalization of the Simmons formalism[43] is necessary to describe the electronic tunnelling through two hemi-spherical surfaces corresponding to the head and tail of two adjacent conductive regions. This generalization allowed us to obtain an expression for the electron tunnelling resistance:[13]

$$R_{tunnel} = \frac{2}{\pi B\gamma \int_x^W \frac{W-z}{z}\exp[-\gamma z]dz} \quad (2)$$

where $W \equiv x + \langle D\rangle$, $\langle D\rangle$ is the average diameter of one pseudo-chain and the parameter $x \equiv x(P,H)$ is the average distance that the electrons must traverse in one tunnel step (associated with a polymer layer between conductive regions). Eqn (2) has no analytical solution and was numerically evaluated using the

Numerical Integration module of SageMath. In the Simmons' formalism γ and B are given by:

$$\gamma = \frac{4\pi}{h}\sqrt{2m\varphi} \quad (3a)$$

$$B = \frac{3e^2}{8\pi h} \quad (3b)$$

where e is the electron charge, m is the effective mass of electron in the filler, φ is the average height of the (rectangular) potential barrier associated with the insulating matrix-filler system and h is the Planck's constant.

Two parameters in eqn (2) and (3a), φ and x, can be, in principle, influenced by H. However, the eventual effect of H on φ must be due to electron spin polarization effects, which are discarded on the basis of the discussion in the previous section. Thus, the present model assumes that φ is independent of H.

Therefore, the magnetoresistance effects are incorporated through the dependence of x with H. Here we shall refer to this as magneto-elastic coupling. The concepts behind it are presented here. By applying the external magnetic field, the magnetic-conductive regions inside a pseudo-chain can become magnetized, that is, a magnetization per unit volume $M(H)$ is induced. The magnetization generates an attractive magnetic interaction among the magnetic-conductive regions. This interaction modifies the distance x, until levelling the elastic force associated with the compression of the polymer insulating layer which separates the conductive regions. Thus, when the SEC is magnetized, a decrease of the spacing between conductive regions is expected. Mathematically, $x = x(M)$ is proposed. In this sense, the magnetic force field acts like a mechanical force field, generating a magnetic stress, P_{mag}, in the direction of H. Bossis and co-workers consider that P_{mag} induces effects on the sample similar to those induced by a mechanical stress, P_{mec}.[5] Hence, it is considered that the total stress in a given direction, P, on a sample under an external mechanical stress and a magnetic field H has two components: the mechanical stress, P_{mec}, and the magnetic stress, P_{mag}. In fact, the SECs present piezo- and magneto-resistivity. The piezoresistive response was modelled in a previous article[13] based on the coupling between the external stimulus (a mechanical stress) and the elastic properties. The model for piezoresistivity was experimentally tested under compression conditions only, but it can be used under compression or elongation without restrictions or modifications. On the other hand, concerning the magnetoresistivity response, the external magnetic field always induces a compression of the material through the magnetic-elastic coupling, not elongations. In magnetoresistance studies, the mechanical stress in the direction of the columns, P_{mec}, is fixed constant (before applying the magnetic field) to an arbitrary value, P^*. That is, $P_{mec} = P^* = \text{constant}$.

$$P = P_{mec} + P_{mag} = P^* + P_{mag} \quad (4)$$

Under the application of P^* and in the absence of P_{mag}, the length of the sample in the direction of P^* is referred to as L^*. Then, subsequent application of H in that direction produces a magnetization M which generates the additional stress in that direction, P_{mag}. P_{mag} represents a change in the total applied stress: in the absence of P_{mag} the pressure on the sample is P^* but it is increased to $P = P^* + P_{mag}$ when $M(H) \neq 0$.

The connection between stress P and x is currently accounted for by the so-called affine assumption where the changes in the microscopic distance, x, under a given stress P, are assumed to be proportional to the changes induced on a macroscopic length of the matrix, y, when P is applied:

$$\frac{x(P)}{x^*} = \frac{y(P)}{y^*} \quad \text{(affine assumption)} \quad (5)$$

where x^* and y^* are the respective lengths when $P_{mag} = 0$ and $P_{mec} = P^*$. Note that y in eqn (5) does not refer to the thickness of the SEC but to the thickness of the polymer matrix in the absence of filler particles. Thus, the affine assumption proposes that magnetic-conductive regions, separated by a layer of the matrix, move along with the matrix. The affine assumption is reasonable in relatively highly cross-linked polymeric matrices where effects of larger deformations of the matrix in the vicinity of very rigid fillers are not considered and the conductive regions (separated by x) follow perfectly the compression motion of the matrix when a stress is applied. The dependence of $y(P)/y^*$ with a given total stress, independently of whether it is magnetic or mechanic, can be parametrized using different models: Hooke Law (linear dependence between y and P), Neo–Hooke model (quadratic dependence),[13] exponential-law[3,16,17,38] or the Moonley–Rivlin model.[13] These models are currently used to fit (mechanical) stress–strain curves in tensile and compression elastic tests. The Hooke and Neo-Hooke models apply to relatively low strains (less than 10%, typically) and do not fit well the mechanic stress–strain curves of PDMS (the matrix of the reference SEC) actually. For these reasons the Hooke Law and the Neo-Hooke model are not considered in the present model. The Mooney–Rivlin model requires one more additional fitting parameter and it is used in a more extended range of strains, *e.g.* 30% deformation. Thus, we assume that the macroscopic elastic behaviour of the PDMS is given by the exponential-law:

$$\frac{dy}{y} = -\frac{dP}{E} \quad (6)$$

where E is the Young's modulus of the matrix (not of the SEC). This model reduces to the Hooke-law in the limit of low stresses in comparison with E. Then, integrations of eqn (5) and (6) under the boundary conditions $y^* \equiv y(= P^* P = P_{mec})$ (that is $P_{mag} = 0$) and $y \equiv y(P) \equiv y(P^* + P_{mag})$ renders:

$$\frac{x}{x^*} = \exp\left(-\frac{P_{mag}}{E}\right) \quad \text{(exponential elastic law)} \quad (7)$$

Thus, x in eqn (2) (Generalized Simmon's Tunnelling model) is related to P_{mag} through eqn (7).

Note that P_{mag} must induce changes in the macroscopic length of the SEC, L, analogous to the changes induced by a mechanical stress, P_{mec}. The magnitude of those changes is discussed at the end of the next section.

The dependence of P_{mag} with H must be considered now. The magnetic force between magnetic three-dimensional regions can be approximately considered as directly proportional to the

product of the magnetic dipole moments of the said magnetic regions if the separation between them is very small compared to the average size of those regions.[44–46] This is the case of the SECs considered here: the separation distance between the conductive regions, x, is in the order of a few nanometers while the average size of the conductive regions is in the order of microns (this is already the case of the reference SEC[13]). Then, the magnetic force will be considered proportional to the product of the magnetic dipole moments of the conductive regions. Taking those regions as having equal average volume and considering that the magnetic dipole moments are proportional to the magnetization of the material per volume unit, $M(H)$:

$$P_{\mathrm{mag}} = \left(\frac{M_s^2}{\Lambda}\right)[\hat{M}(H)]^2 \tag{8}$$

where Λ is a geometrical–morphological constant, M_s the saturation magnetization of the filler material and $\hat{M}$ is the normalized magnetization of the filler per volume units ($\hat{M} = M(H)/M_s$, with $-1 \leq \hat{M} \leq 1$).

Thus, from eqn (4)–(8), the dependence of x with H is obtained:

$$x(H) = x^* \exp\left(-\frac{[\hat{M}(H)]^2}{K}\right) \tag{9}$$

where $K \equiv \Lambda E/M_s^2$ is an adjustable constant. Note that the parameter K plays an analogous role concerning P_{mag} than E to P_{mec}: at a given P_{mag} the larger K renders smaller deformations.

The expression for x provided by eqn (9) is used in eqn (2) for predicting the dependence of R_{tunnel} with H. Since the parameters N, n, $R_{\mathrm{E-CR}}$ and R_{CR} are considered as independent of H in the present model, the following expression for the percentage magnetoresistance change can be obtained:

$$\begin{aligned} MR_{\%}(H) &\equiv \left[\frac{R(P^*,H) - R(P^*,H=0)}{R(P^*,H=0)}\right] \times 100 \\ &= \left[\frac{R_{\mathrm{tunnel}}(P^*,H) - R_{\mathrm{tunnel}}(P^*,H=0)}{R_o^*}\right] \times 100 \end{aligned} \tag{10}$$

where $R_o^* \equiv R(P^*, H = 0)$. The present model requires the determination of the normalized magnetization curve of the filler, $\hat{M}(H)$, and then to adjust experimental data of $MR_{\%}(H)$ in order to determine the two adjustable (fitting) parameters: ($x^*\gamma$) and K. The cases of SECs in superparamagnetic states and blocked states (presenting magnetic hysteresis) are separately discussed in the next sections.

4 Results and discussion

4.1 Experimental magnetic and magnetoresistance behaviour of the reference superparamagnetic SEC (Fe_3O_4[Ag]–PDMS)

The normalized magnetization curves, $\hat{M}(H)$, for the superparamagnetic state are generally well-described by a Langevin function, $\mathscr{L}(H)$:[47]

$$\hat{M}(H) = \mathscr{L}(H) = \coth(\hat{H}) - 1/\hat{H} \tag{11}$$

where the reduced magnetic field is defined as $\hat{H} \equiv H/H^{\ddagger}$ and $H^{\ddagger}$ is a characteristic magnetic field, specific for each material.

For the reference SEC, the filler particles (Fe_3O_4[Ag] microparticles) follows the behaviour given by eqn (11) as shown in Fig. 3. In that figure, the solid line corresponds to fits of $M(H) = \hat{M}(H)M_s$, using eqn (11). From this fit, the parameters $H^{\ddagger} = (420 \pm 9)$ Oe and $M_s = (71.0 \pm 0.4)$ kA m^{-1} are obtained. Note, however, that the convergence of the experimental data to a linear dependence of M with H (instead of reaching a plateau) at large positive or negative fields indicates the presence of some paramagnetic component, associated with metallic silver, which represents a small contribution and is not taken into account.

In the magnetoresistance experiments, the mechanical stress in the direction of the electrical current (and of the pseudo-chains) is always kept fixed to a given arbitrary value ($P^* \approx 75$ kPa in the reference SEC). When a magnetic field is applied in that direction, the resistance R changes until stabilization, as shown in Fig. 4(a). The relaxation process can be modelled as mono-exponential

$$\begin{aligned} MR_{\%}(H,t) = [MR_{\%}(H=0) - MR_{\%}(H)]\exp\left(-\frac{t}{\tau_R}\right) \\ + MR_{\%}(H) \end{aligned} \tag{12}$$

The observed characteristic magnetoresistance transient time, τ_R, is dependent on the magnitude of the change in the magnetic field, although typically around 3–5 seconds for the reference SEC (in accordance with the values reported in the literature[48–50]). The value of τ_R is not significantly influenced by instrumental factors (see Materials and methods) but rather seems to be an intrinsic physical property of the SEC. Moreover, τ_R is very similar to the observed characteristic elastic relaxation time, τ_E, which is the observed characteristic mono-exponential relaxation time for obtaining a stabilized stress after applying a given strain (see Fig. 4(b)). This observation is in agreement with the physical picture behind our model: the magnetic field induces a magnetic pressure which changes the microscopic and macroscopic dimensions of the sample (x and L, respectively), requiring a

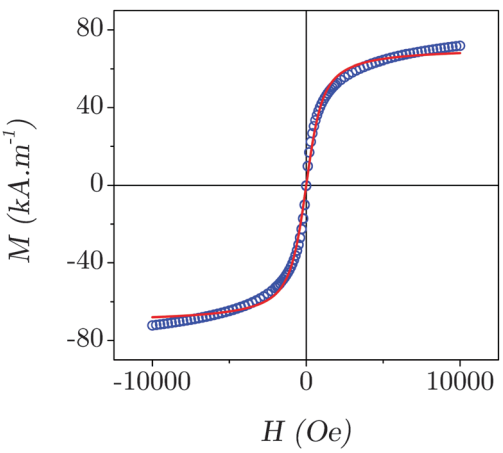

Fig. 3 Magnetization curve of the filler Fe_3O_4[Ag] at 25 °C. The solid line corresponds to the fits by eqn (11).

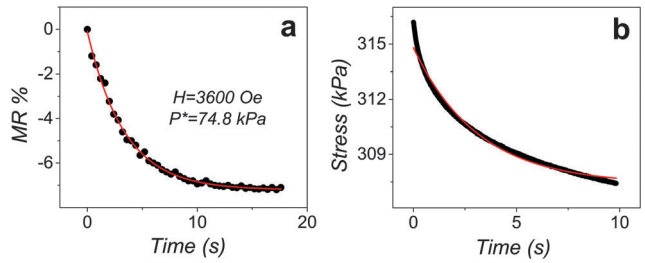

Fig. 4 (a) Change in the electrical resistance R after application of a magnetic field, H, for the reference SEC. (b) Change in the mechanical stress, P, after applying a fixed strain (30%) on the reference SEC. In both panels, the solid line corresponds to a mono-exponential relaxation process $S(H,t) = [S(H = 0) - S(H)]\exp(-t/\tau_S) + S(H)$ with S = stress or $MR_{\%}$.

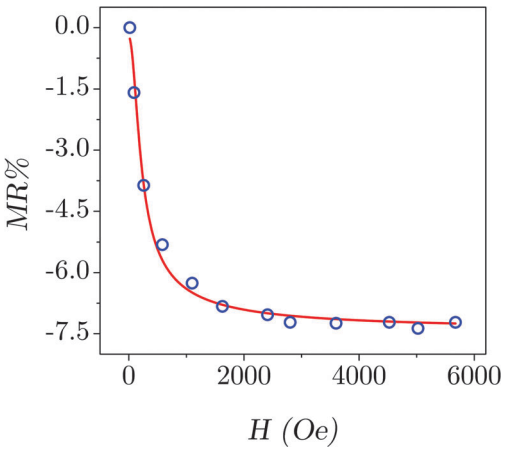

Fig. 5 MR response of the SEC Fe_3O_4[Ag]–PDMS 4.2%. The solid line corresponds to the constitutive model given by eqn (1)–(11).

time of the order of τ_E for reaching stabilization of properties such as the electrical resistance R (associated with x with a time τ_R) or the stress–strain curves (associated with L with a time τ_E). The experimental similitude between τ_R and τ_E is in agreement with that picture. It is worth highlighting that τ_R and τ_E depend on the viscoelastic properties of the matrix and filler–matrix interaction. For example, the relatively large τ_R recently reported for a strain sensor based on ultra-soft elastomers[48] could be due to the lower force required for quick re-establishment of the percolating network.

The stabilized values of R at each value of H were registered. The percentage magnetoresistance, $MR_{\%}$, defined in eqn (10) (with $R_o^* \approx 1.95\ \Omega$) is shown as a function of H in Fig. 5. The solid line corresponds to the fit made by the constitutive equations of the described model. The quality of the fit is very good ($R^2 = 0.997$). The values $(x^*\gamma) = (9.4 \pm 0.7)$ and $K = (93 \pm 9)$ are recovered from the fit. Since the model assumes that the potential barrier, φ, is not influenced by H, then the value recently reported for γ of Ag–PDMS systems, $\gamma = 10\ nm^{-1}$, can be reasonably used as a good estimation.[13,24] Using that value, then $x^* = 0.9$ nm is calculated.

The maximum magnetic stress is reached when $(\hat{M})^2 = 1$ (saturation of the magnetization). The predicted value is $P_{mag}^{max} = E/K$. For composites in PDMS $E \approx$ 700–800 kPa, dependent on the degree of cross-linking.[3,51] Then, in the reference SEC it is predicted that $P_{mag}^{max} \approx$ 7–9 kPa. The magnitude of the maximum achievable microscopic magnetic strain is given by $(1 - x/x^*)$ evaluated for $(\hat{M})^2 = 1$. That value of microscopic strain equals $1 - \exp(-1/K)$ in the model [see eqn (9) with $(\hat{M})^2 = 1$]. Using the recovered value of K ($K = 93$) a maximum magnetic microscopic strain of 1% is predicted in the reference SEC.

The issue concerning the macroscopic deformation in the reference SEC under P_{mag} is now addressed. Under the affine assumption, the microscopic strain is equal to the macroscopic strain of the matrix. A maximum strain of 1% was calculated (above paragraph), that is, a polymer matrix without filler particles must be compressed less than 1% if a mechanical pressure with equal value to the magnetic pressure is applied. Since the Young's modulus of the SEC in the direction parallel to H, $E_{\parallel}$, is slightly larger than E,[3,16,17,52] even smaller strains are expected in the SEC. For instance, in the reference SEC $L^* \sim$ 1 mm, then the above considerations predict that a change lower than 10 μm must occur at large magnetic fields, which is not detected when the SEC is placed in the sample's holder.

4.2 Simulations of the magnetoresistance response for superparamagnetic SECs

Simplifying the analysis, the Simmons formalism for metallic parallel plates was considered in order to simulate the curves of $R_{tunnel}(H)/R^*$, with $R^* \equiv R_{tunnel}(P_{mag} = P^*, P_{mag} = 0) \equiv R_{tunnel}(P_{mag} = P^*, M = 0)$:[43,53]

$$R_{tunnel}(x) \propto x\exp(x\gamma) \quad (13)$$

Hence, the model provides the following simplified expression:

$$\frac{R_{tunnel}}{R^*} = \exp\left\{x^*\gamma\left[\exp\left(-\frac{[\hat{M}^2(H)]^2}{K}\right) - 1\right] - \frac{[\hat{M}(H)]^2}{K}\right\} \quad (14)$$

The effect of $H^{\ddagger}$, K and $(x^*\gamma)$ on $R_{tunnel}(H)/R^*$ was evaluated by simulating curves using eqn (14) (Fig. 6).

These simulations show that the sensitivity in the magnetoresistance response (MR response) can be increased in several ways:

(i) Lowering the value of K, since sensitivity to H decreases when K increases. Lower K corresponds to higher M_s (stronger magnetic particles induces larger P_{mag}) or lower E (a softer matrix is easier to compress under a given H). The K values used for the simulations correspond to M_s in the range 100–150 kA m^{-1} (easy to achieve in many magnetic materials) and values of E associated with natural and synthetic rubber and epoxy resins.[54]

(ii) Increasing $x^*\gamma$. In fact, if $x^* \ll \gamma^{-1}$ (low $x^*\gamma$) then conduction is relatively high (low values of R) and difficult to modify by a magnetic field: the material remains with high conductivity and low magnetoresistivity effects are predicted. The values of $x^*\gamma$ used in the simulations are experimentally achievable by changing the preparation conditions of the SEC or changing the chemical nature of the filler, changing the preparation conditions of the SEC and the value of P^*.

The MR curves obtained with our model show an inflection point (see Fig. 6), whose position is easily found numerically. It can be shown that the inflection point is shifted to lower values

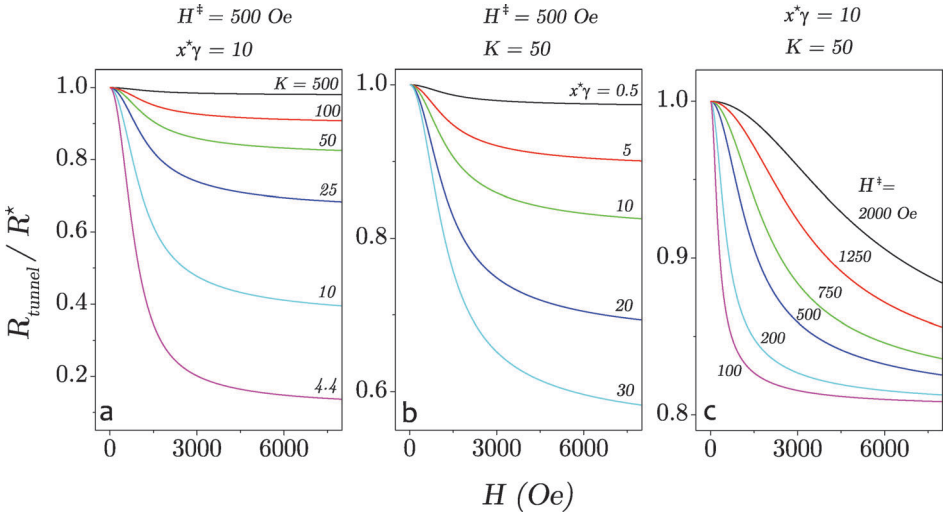

Fig. 6 Simulated curves of R_{tunnel}/R^{*} as a function of H. (a) Effect of K with $H^{\ddagger}$ = 500 Oe and $x^{*}\gamma$ = 10. (b) Effect of $x^{*}\gamma$ with K = 50 and $H^{\ddagger}$ = 500 Oe. (c) Effect of $H^{\ddagger}$ with K = 50 and $x^{*}\gamma$ = 10.

of H for higher values of x^{*}, φ and M_s and lower values of E and $H^{\ddagger}$ (the latter is clearly seen in Fig. 6(c)).

The application of H in the opposite direction give a symmetrical MR response, *i.e.* $R_{tunnel}(H) = R_{tunnel}(-H)$ (not shown). This is a direct consequence of the symmetry of the magneto-elastic coupling phenomenon when H is collinear to columnar structures.

4.3 Extension of the model to systems with blocked magnetization

The model can be used to predict the MR response for anisotropic SEC systems with columnar structures formed by fillers presenting blocked magnetic states with magnetic hysteresis, as long as there is no filler–matrix adhesion (no Mullins effect). Hysteresis in the MR response is expected as a consequence of the magnetic hysteresis, through the dependence of R_{tunnel} with $\hat{M}(H)$. Thus, the first step is to simulate the magnetization curves for systems with blocked magnetization and then to use it to simulate the magnetoresistance as a function of H. Several models can be used to describe blocked magnetization curves, $\hat{M}(H)$, like the Jiles–Atherton model.[55] A function widely used for fitting experimentally blocked magnetization curves is:[56–58]

$$\hat{M}(\hat{H}) = \frac{2}{\pi}\tan^{-1}\left[(\hat{H}+\zeta)\tan\left(\frac{\pi\Theta}{2}\right)\right] \qquad (15)$$

where M_r is the remnant magnetization, $\Theta = M_r/M_s$ is the squareness of the magnetization curve, H_c is the coercive field, the reduced field is $\hat{H} \equiv H/H_c$, and the reduced magnetization is $\hat{M} \equiv M/M_s$ (as defined before). eqn (15) implicitly assumes that the magnetization characteristic response of the particles is in a steady state. In that expression, $\zeta = -1$ if $\frac{dH}{dt} > 0$ and $\zeta = 1$ if $\frac{dH}{dt} < 0$, that is, $\zeta = -1(+1)$ correspond to the magnetization (de-magnetization) curve, respectively.

Fig. 7(a) shows the simulated magnetization loops using eqn (15) for different values of H_c and fixed M_s and Θ, where the solid (dotted) line corresponds to $\zeta = -1(+1)$. This notation is retained in the following figures (see a zoom in Fig. 7(b)). Fig. 7(c) shows the effect of H_c on simulated curves R_{tunnel}/R^{*} *vs.* H for SEC systems displaying the magnetization loops of Fig. 7(a). All the R_{tunnel}/R^{*} curves converge asymptotically to the same value $\frac{R_\infty}{R^{*}}$ for $H \to \pm\infty$, which, as in the case of the superparamagnetic filler, depends only on M_s, K and the energetic-structural parameter $(x^{*}\gamma)$ is given by

$$\frac{R_{tunnel}}{R^{*}} \xrightarrow{H\to\pm\infty} \frac{R_\infty}{R^{*}} = \exp\left\{x^{*}\gamma\left[\exp\left(-\frac{1}{K}\right)-1\right]-\frac{1}{K}\right\} \qquad (16)$$

On the other hand, note that while superparamagnetic fillers induce a monotonic decrease of R_{tunnel} with H, the blocked magnetization induces the presence of an absolute maximum in the magnetoresistance response of the SEC as a function of H, in $H = \pm H_c$. These maxima are clearly observed in Fig. 7(d), a zoom of Fig. 7(c), where the arrows indicate the maxima at $H = \pm H_c$. This behaviour is a consequence of the fact that the model considers that $P_{mag}(H)$ increases with $(\hat{M})^2$, then R_{tunnel} is a decreasing function of $(\hat{M})^2$. Consider for instance the curves with $\zeta = -1$ and $H > 0$ (H is increased). In this case, $(\hat{M})^2 = (M_r/M_s)^2$ and $R_{tunnel}/R^{*} < 1$ for $H = 0$. Then $(\hat{M})^2$ decreases from $(\hat{M})^2 = (M_r/M_s)^2$ at $H = 0$ to $(\hat{M})^2 = 0$ at $H = H_c$, hence $R_{tunnel}/R^{*} \leq 1$ in the range $0 \leq H \leq H_c$. When $H = H_c$, $(\hat{M})^2 = 0$ and $R_{tunnel}/R^{*} = 1$, the maximum value. If now H is increased above H_c a turn-over of the response appears since $(\hat{M})^2$ increases again with the consequence of decreasing R_{tunnel}/R^{*}. Therefore, the effect of increasing H_c is to shift the position of the turn-over in the magnetoresistance response.

The effect of changing Θ on the magnetization loops is presented in Fig. 8(a) and (b). The variation of R_{tunnel}/R^{*} *vs.* H for that case is shown in panels c and d [fixing K, $(x^{*}\gamma)$, M_s and H_c]. Increasing Θ in those curves implies increasing M_r and

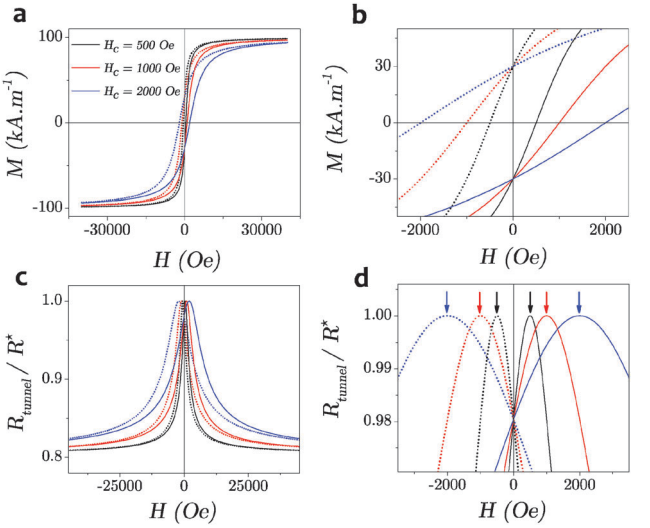

Fig. 7 (a) Simulated magnetization loops using eqn (15) with M_s = 100 kA m^{-1}, Θ = 0.3 and H_c = 500, 1000 and 2000 Oe. The solid lines correspond to the magnetization, dH/dt > 0, and the dotted one to the de-magnetization, dH/dt < 0. (b) Zoom of the panel (a) that clearly show that all the M(H) loops have the same remanence, but different coercivity. (c) Effect of H_c on simulated curves R_{tunnel}/R^* as a function of H with K = 50, $x^*\gamma$ = 10, M_s = 100 kA m^{-1}, Θ = 0.3 and H_c = 500, 1000 and 2000 Oe. (d) Zoom of the panel (c) where the arrows indicate the maxima at $H = \pm H_c$.

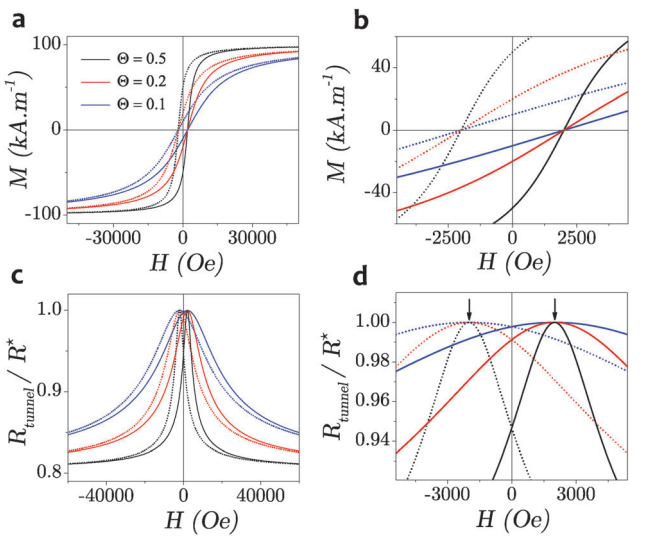

Fig. 8 (a) Simulated magnetization loops using eqn (15) with M_s = 100 kA m^{-1}, H_c = 2000 and Θ = 0.1, 0.2 and 0.5. (b) Zoom of the panel (a) that clearly shows that all the M(H) loops have the same coercivity, but different remanence. (c) Effect of Θ on simulated curves R_{tunnel}/R^* as a function of H with K = 50, $x^*\gamma$ = 10, M_s = 100 kA m^{-1}, H_c = 2000 and Θ = 0.1, 0.2 and 0.5. (d) Zoom of panel (c); the arrows indicate the maxima at $H = \pm H_c$.

therefore $\hat{M}(H = 0)$. Thus, R_{tunnel}/R^* becomes more sensitive to H when Θ (or M_r) increases, that is, a more abrupt variation is observed [$|d(R_{tunnel}/R^*)/dH|$ increases with Θ, except at $H = \pm H_c$ where it is zero as discussed in the previous paragraph]. The response converges to the same value, $R_{tunnel}/R^* \approx 0.8$, when $H \to \pm\infty$ since that value does not depend on Θ.

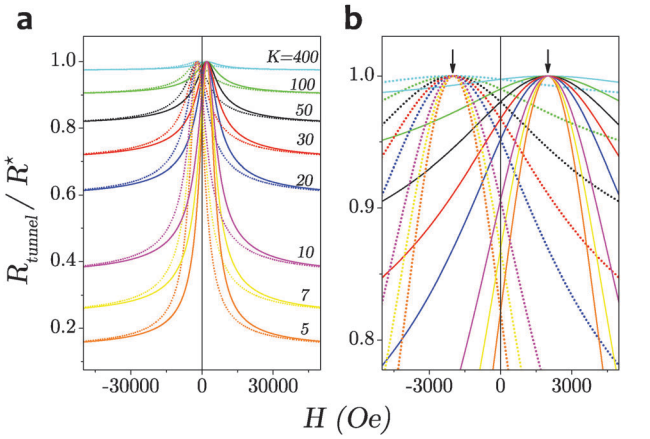

Fig. 9 (a) Effect of K on simulated curves R_{tunnel}/R^* as a function of H with M_s = 100 kA m^{-1}, $x^*\gamma$ = 10, Θ = 0.3 (M_r = 30 kA m^{-1}) and H_c = 2000 Oe. (b) Zoom of the panel (a) where the arrows indicate the maxima at $H = \pm H_c$.

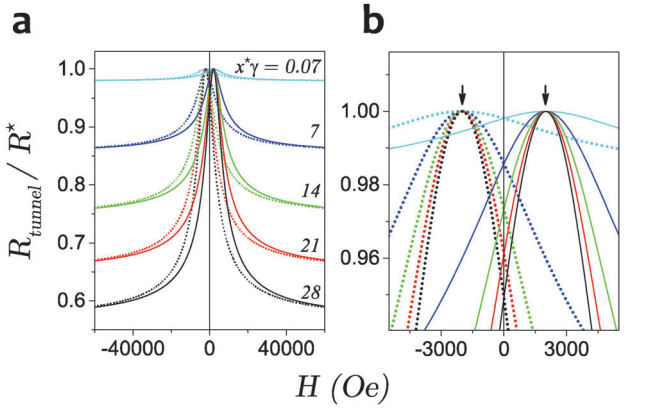

Fig. 10 (a) Effect of $x^*\gamma$ on simulated curves R_{tunnel}/R^* as a function of H with M_s = 100 kA m^{-1}, K = 50, Θ = 0.3 (M_r = 30 kA m^{-1}) and H_c = 2000 Oe. (b) Zoom of the panel (a) where the arrows indicate the maxima at $H = \pm H_c$.

Fig. 9(a) shows the effect of K on simulated curves (R_{tunnel}/R^*)(H) with fixed values of M_s, ($x^*\gamma$), Θ and H_c. Fig. 9(b) shows a zoom of the simulated curves, where again, the arrows indicate the maxima at $H = \pm H_c$. In this case, each curve converges to a different value at large H.

Finally, Fig. 10(a) shows the effect of ($x^*\gamma$) on simulated curves (R_{tunnel}/R^*) as a function of H with fixed values of M_s, K, Θ and H_c. Fig. 10(b) shows a zoom of the simulated curves where, again, the arrows indicate the maxima at $H = \pm H_c$. In this case, each curve converge to a different value at large H.

If only the magnetization curve at positive fields is considered, an inflection point and a maximum at $H = H_c$ are clearly observed. This inflection point and maximum are observed in a recent report by Pang *et al.*[59] actually, for composites prepared with ferromagnetic carbonyl iron particles, flake graphite powder and a polyurethane matrix.

5. Conclusions

The presented model accounts for the main features concerning magnetoresistivity in SECs. Very good fits of experimental

data for the reference SEC are provided. The model can be applied to systems in superparamagnetic or blocked states. The main issue in these kinds of systems is to answer why very large magnetoresistivity effects can be obtained. The answer proposed by the model is that electron tunnelling can be significantly enhanced if: (a) magnetization (M) is large enough to generate a moderate but non-negligible magnetic stress (P_{mag}), (b) if P_{mag} is able to induce microscopic decrease of tunnelling distances (x), (c) if those distances are not too short in comparison with the characteristic tunnelling distance. The aspects (a) and (b) are related to the parameter K of the model, which is connected not only to the capability of inducing a magnetic stress through the parameters Λ and M_s but also to the hardness of the material to be deformed by that stress through the Young's modulus of the matrix, E. The aspect (c) is typical of electron tunnelling: if the distance for tunnelling is too short then conductivity is relatively high and cannot be easily changed by external forces. The model accounts for the physics behind the magneto-elastic coupling, by using only two parameters: (γx^*) and K. The conjunction of the above factors causes that even a microscopic decrease of only 1% in x can induce about 10% of magnetoresistive changes depending on (γx^*), while for the same (γx^*), 10% of microscopic strain generates 60% of magnetoresistivity changes (see Fig. 6). The model assumes the condition of TEA, that is, there is connectivity (percolation) but that connectivity appears only in one direction. If the concentration of particles is in a window range that ensures those conditions, then no large effects of filler's concentration on the magnetoresistivity are predicted. In other words, concentration plays a significant role in generating these systems, but no relevant concentration effects are expected as far as TEA conditions are presented.

Acknowledgements

RMN and PIT are research members of the National Council of Research and Technology (CONICET, Argentina). The authors gratefully acknowledge the stimulating discussions with Dr Robert D. McGinty (Mercer Engineering Research Center, USA). Financial support was received from UBA (UBACyT projects 2012–2015, number 20020110100098 and 2011–2014 number 20020100100741), and from the Ministry of Science, Technology, and Innovation (MINCYT-FONCYT, Argentina, PICT 2011-0377). The Low-Temperatures Laboratory (Department of Physics, FCEyN, UBA) is gratefully acknowledged for providing the facilities used to implement the device which generates the structured materials.

References

1 I. Bica, Y. D. Liu and H. J. Choi, *J. Ind. Eng. Chem.*, 2013, **19**, 394–406.
2 J. L. Mietta, G. Jorge, O. E. Perez, T. Maeder and R. M. Negri, *Sens. Actuators, A*, 2013, **192**, 34–41.
3 J. L. Mietta, M. M. Ruiz, P. S. Antonel, O. E. Perez, A. Butera, G. Jorge and R. M. Negri, *Langmuir*, 2012, **28**, 6985–6996.
4 M. Yu, B. Ju, J. Fu, S. Liu and S.-B. Choi, *Ind. Eng. Chem. Res.*, 2014, **53**, 4704–4710.
5 N. Kchit, P. Lancon and G. Bossis, *J. Phys. D: Appl. Phys.*, 2009, **42**, 105506.
6 G. Filipcsei, I. Csetneki, A. Szilágyi and M. Zrínyi, *Oligomers-Polymer Composites-Molecular Imprinting*, Springer, 2007, pp. 137–189.
7 Z. Varga, G. Filipcsei and M. Zrínyi, *Polymer*, 2005, **46**, 7779–7787.
8 Z. Varga, G. Filipcsei and M. Zrínyi, *Polymer*, 2006, **47**, 227–233.
9 L. Nikitin, G. Stepanov, L. Mironova and A. Gorbunov, *J. Magn. Magn. Mater.*, 2004, **272**, 2072–2073.
10 L. Nikitin, G. Stepanov, L. Mironova and A. Samus, *J. Magn. Magn. Mater.*, 2003, **258**, 468–470.
11 L. Nikitin, D. Korolev, G. Stepanov and L. Mironova, *J. Magn. Magn. Mater.*, 2006, **300**, e234–e238.
12 J. L. Mietta, R. M. Negri and P. I. Tamborenea, *J. Phys. Chem. C*, 2014, **118**, 20594–20604.
13 J. L. Mietta, P. I. Tamborenea and R. M. Negri, *Soft Matter*, 2016, **12**, 422–431.
14 J. L. Mietta, G. Jorge and R. M. Negri, *Smart Mater. Struct.*, 2014, **23**, 085026.
15 M. M. Ruiz, M. Claudia Marchi, O. E. Perez, G. E. Jorge, M. Fascio, N. D'Accorso and R. Martín Negri, *J. Polym. Sci., Part B: Polym. Phys.*, 2015, **53**, 574–586.
16 M. M. Ruiz, J. L. Mietta, P. S. Antonel, O. E. Pérez, R. M. Negri and G. Jorge, *J. Magn. Magn. Mater.*, 2013, **327**, 11–19.
17 P. S. Antonel, G. Jorge, O. E. Perez, A. Butera, A. G. Leyva and R. M. Negri, *J. Appl. Phys.*, 2011, **110**, 043920.
18 D. S. Wood and P. J. Camp, *Phys. Rev. E: Stat., Nonlinear, Soft Matter Phys.*, 2011, **83**, 011402.
19 G. Pessot, R. Weeber, C. Holm, H. Löwen and A. M. Menzel, *J. Phys.: Condens. Matter*, 2015, **27**, 325105.
20 S. Huang, G. Pessot, P. Cremer, R. Weeber, C. Holm, J. Nowak, S. Odenbach, A. M. Menzel and G. K. Auernhammer, *Soft Matter*, 2016, **12**, 228–237.
21 R. Weeber, S. Kantorovich and C. Holm, *J. Chem. Phys.*, 2015, **143**, 154901.
22 D. Ivaneyko, V. Toshchevikov, D. Borin, M. Saphiannikova and G. Heinrich, *Macromol. Symp.*, 2014, pp. 96–107.
23 F. Du, J. E. Fischer and K. I. Winey, *Phys. Rev. B: Condens. Matter Mater. Phys.*, 2005, **72**, 121404.
24 M. Amjadi, A. Pichitpajongkit, S. Lee, S. Ryu and I. Park, *ACS Nano*, 2014, **8**, 5154–5163.
25 N. Hu, H. Fukunaga, S. Atobe, Y. Liu and J. Li, *Sensors*, 2011, **11**, 10691–10723.
26 N. Hu, Y. Karube, C. Yan, Z. Masuda and H. Fukunaga, *Acta Mater.*, 2008, **56**, 2929–2936.
27 E. Holm, J. Williamson and R. Holm, *Electric Contacts: Theory and Application*, Springer, Berlin Heidelberg, 2010.
28 G. Samsonov, *Handbook of the Physicochemical Properties of the Elements*, Springer, US, 2012.

29 X. Kou, W. Wang, X. Fan, L. R. Shah, R. Tao and J. Q. Xiao, *J. Appl. Phys.*, 2010, **108**, 083901.
30 S. Pramanik, C.-G. Stefanita, S. Patibandla, S. Bandyopadhyay, K. Garre, N. Harth and M. Cahay, *Nat. Nanotechnol.*, 2007, **2**, 216–219.
31 Z. Fan, P. Li, E. Jiang and H. Bai, *Carbon*, 2012, **50**, 4470–4475.
32 K. Z. Suzuki, Y. Shibuya, T. Niizeki, H. Yanagihara and E. Kita, *IEEE Trans. Magn.*, 2014, **50**, 1–4.
33 M. Pauly, J.-F. Dayen, D. Golubev, J.-B. Beaufrand, B. P. Pichon, B. Doudin and S. Bégin-Colin, *Small*, 2012, **8**, 108–115.
34 T. Pham, S. Miwa, D. Bang, T. Nozaki, F. Bonell, E. Tamura, N. Mizuochi, T. Shinjo and Y. Suzuki, *Solid State Commun.*, 2014, **183**, 18–21.
35 J. Dugay, R. P. Tan, A. Meffre, T. Blon, L.-M. Lacroix, J. Carrey, P. F. Fazzini, S. Lachaize, B. Chaudret and M. Respaud, *Nano Lett.*, 2011, **11**, 5128–5134.
36 J. Montes, F. Cuevas, J. Cintas and P. Urban, *Appl. Phys. A: Mater. Sci. Process.*, 2011, **105**, 935–947.
37 N. Kchit and G. Bossis, *J. Phys. D: Appl. Phys.*, 2009, **42**, 105505.
38 R. M. Negri, S. D. Rodriguez, D. L. Bernik, F. V. Molina, A. Pilosof and O. Perez, *J. Appl. Phys.*, 2010, **107**, 113703.
39 S. B. Bubenhofer, C. M. Schumacher, F. M. Koehler, N. A. Luechinger, G. A. Sotiriou, R. N. Grass and W. J. Stark, *ACS Appl. Mater. Interfaces*, 2012, **4**, 2664–2671.
40 H. Gu, X. Zhang, H. Wei, Y. Huang, S. Wei and Z. Guo, *Chem. Soc. Rev.*, 2013, **42**, 5907–5943.
41 E. Y. Tsymbal and I. Zutic, *Handbook of Spin Transport and Magnetism*, CRC press, 2011.
42 C. Chappert, A. Fert and F. N. Van Dau, *Nat. Mater.*, 2007, **6**, 813–823.
43 J. G. Simmons, *J. Appl. Phys.*, 1964, **35**, 2655–2658.
44 A. Biller, O. Stolbov and Y. L. Raikher, *J. Appl. Phys.*, 2014, **116**, 114904.
45 T. Liu, X. Gong, Y. Xu, S. Xuan and W. Jiang, *Soft Matter*, 2013, **9**, 10069–10080.
46 D. Vokoun, M. Beleggia, L. Heller and P. Šittner, *J. Magn. Magn. Mater.*, 2009, **321**, 3758–3763.
47 M. Knobel, W. Nunes, L. Socolovsky, E. De Biasi, J. Vargas and J. Denardin, *J. Nanosci. Nanotechnol.*, 2008, **8**, 2836–2857.
48 M. Amjadi, K.-U. Kyung, I. Park and M. Sitti, *Adv. Funct. Mater.*, 2016, **26**, 1678–1698.
49 T. Yamada, Y. Hayamizu, Y. Yamamoto, Y. Yomogida, A. Izadi-Najafabadi, D. N. Futaba and K. Hata, *Nat. Nanotechnol.*, 2011, **6**, 296–301.
50 C. Mattmann, F. Clemens and G. Tröster, *Sensors*, 2008, **8**, 3719–3732.
51 Y. Zheng, *Liquid Plug Dynamics in Pulmonary Airways*, ProQuest, 2008.
52 C. Hui and D. Shia, *Polym. Eng. Sci.*, 1998, **38**, 774–782.
53 H. Zhao and J. Bai, *ACS Appl. Mater. Interfaces*, 2015, **7**, 9652–9659.
54 J. Mark, *Physical Properties of Polymers Handbook*, Springer, New York, 2007.
55 D. Jiles and D. Atherton, *J. Magn. Magn. Mater.*, 1986, **61**, 48–60.
56 Y. Zhang, L. Pan, H. Zhu, W. Wang, L. R. Shah, X. Fan and J. Q. Xiao, *J. Appl. Phys.*, 2010, **107**, 09C305.
57 S. Duhalde, M. Vignolo, F. Golmar, C. Chiliotte, C. R. Torres, L. Errico, A. Cabrera, M. Renteria, F. Sanchez and M. Weissmann, *Phys. Rev. B: Condens. Matter Mater. Phys.*, 2005, **72**, 161313.
58 M. B. Stearns and Y. Cheng, *J. Appl. Phys.*, 1994, **75**, 6894–6899.
59 H. Pang, S. Xuan, T. Liu and X. Gong, *Soft Matter*, 2015, **11**, 6893–6902.